Int. J. Heat Mass Transfer. Vol. 32, No. 10, pp. 1865–1878, 1989
Printed in Great Britain

0017–9310/89 $3.00 + 0.00

Water vapour diffusion and condensation in fibrous insulations

N. E. WIJEYSUNDERA, M. N. A. HAWLADER and Y. T. TAN
Department of Mechanical and Production Engineering, National University of Singapore, 10 Kent Ridge Crescent, Singapore 0511

(*Received* 14 *July* 1988 *and in final form* 22 *February* 1989)

Abstract—An experimental study of the diffusion and condensation of water vapour in fibreglass slab insulations is reported. In the first series of experiments, water is sprayed on the hot face of the slab and it is tested in a heat flow meter apparatus. In the second set of experiments, one of the faces of the slab is exposed to a warm and humid ambient and the other face is maintained at a low temperature. Simple analytical models are developed for the quasi-steady phase of the condensation process in the two experiments. The predicted temperature distribution, heat flux and vapour flux agree well with the measured quantities.

INTRODUCTION

THE OPERATION of low-temperature insulation systems in environments of high ambient humidity and temperature, as it is in the tropics, presents special problems. With porous insulation materials like fibreglass, the diffusion of moist air can lead to condensation of water within the insulation material. This process could be initiated by a damaged or a poorly installed vapour barrier and often this situation is discovered only when irreversible damage has been done to the insulation. The location of insulated chilled water pipes and cold air ducts in areas that experience very moist ambient conditions during heavy rain may also lead to moisture ingress into the insulation. The long-term effect of the condensation of moisture in the insulation is the corrosion of the insulated duct surface [1] and the eventual destruction of the insulation system.

There has been considerable interest in the effect of moisture on thermal insulation, particularly in relation to the insulation of buildings in temperate climates. Early work on the subject was reported by Jespersen [2], Joy [3] and Woodside [4]. Jespersen [2] used a steady-state heat flow method to measure the thermal conductivity of glass fibre slabs while Joy [3] employed the transient heat flow method to obtain similar results. The experimental work of Woodside [4] was also based on the transient thermal probe. Due to the relatively long time involved in steady-state methods of measurement, there is significant moisture redistribution within the insulation during the experiment as pointed out by Langlais *et al.* [5]. This effect is believed to be less pronounced when the transient probe is used because of the short time required for the measurement. This issue was investigated in an experimental study [11], where both methods were used on insulation slabs with the same level of moisture. Thomas *et al.* [6] used a guarded hot plate apparatus to measure the thermal conductivity of fibrous insulations with very high moisture levels. The moisture gain by spray-applied insulation slabs from the surroundings was investigated by Modi and Benner [8] using a heat flow meter method.

The modelling of the diffusion and condensation of water vapour in porous insulations has received some attention in the recent literature. Ogniewicz and Tien [12] considered the vapour transport processes in a porous slab. The quasi-steady phase of the heat and mass transfer processes was modelled. Motakef and El-Masri [13] analysed a similar physical situation, considering two separate quasi-steady phases of the transport process. A numerical solution of the transport equations including phase change was obtained by Vafai and Sarkar [14]. In this case the transient equations were solved for three types of boundary conditions.

In the present paper, an experimental study of the water vapour diffusion and condensation processes in fibreglass insulation slabs is reported. Two sets of experiments have been carried out. In the first series of tests, water is sprayed on to the hot face of the insulation slab, as in the tests reported by Langlais and Klarsfeld [7]. In the second series of experiments, the hot face of the insulation slab is exposed to a warm humid ambient. Simple analytical models are developed for the quasi-steady phase of the transport processes with the above boundary conditions.

In the next section of the paper, the experimental arrangement is described. The analytical models and the results are presented in subsequent sections.

EXPERIMENTAL ARRANGEMENT AND PROCEDURE

The purpose of the present experimental programme was to study the thermal properties of insulations when vapour diffusion and condensation occur

NOMENCLATURE

a	constant in Clausius–Clapeyron relationship [K^{-1}]
c	mean specific heat capacity of slab [kJ kg^{-1} K^{-1}]
C	concentration of water vapour [kg kg(dry air)$^{-1}$]
$\bar{C}$	constant in Clausius–Clapeyron relationship [kg kg^{-1}]
$C^*(T)$	saturation concentration at temperature T [kg kg(dry air)$^{-1}$]
D_a	diffusivity of water vapour–air mixture [m^2 s^{-1}]
D_0	diffusivity of vapour in slab [m^2 s^{-1}]
$g(T)$	function in Clausius–Clapeyron relationship [kg kg^{-1}]
h_a	heat transfer coefficient from ambient to insulation surface [W m^{-2} K^{-1}]
h_m	mass transfer coefficient from ambient to insulation surface [kg m^{-2} s^{-1}]
h_{fg}	specific enthalpy during change of phase [kJ kg^{-1}]
k	thermal conductivity of dry slab [W m^{-1} K^{-1}]
k_e	equivalent local thermal conductivity of slab with condensation [W m^{-1} K^{-1}]
L	thickness of slab [m]
L_d	thickness of dry region of slab [m]
L_w	thickness of wet region of slab [m]
q	heat flux through slab [W m^{-2}]
t	time [s]
$T(z)$	temperature distribution in slab [K]
T_0	reference temperature [K]
T_a	ambient temperature [K]
z	distance [m].

Greek symbols

Γ	condensation rate [kg m^{-3} s^{-1}]
ε_v	void fraction
ρ	mean local density of slab [kg m^{-3}]
ρ_a	local density of moist air [kg m^{-3}]
τ	tortuosity factor
$\phi(z)$	vapour mass flux in slab [kg m^{-2} s^{-1}].

Subscripts

1	hot face of slab
2	cold face of slab
a	ambient conditions
c	conditions at the dry–wet interface.

in the slab. The effect of two different and practically relevant boundary conditions at the hot face of the slab was investigated. This required the design of two experimental arrangements. The first experimental set-up was similar to a conventional heat flow meter apparatus [9]. This test set-up had to be modified to simulate the situation where moisture is absorbed from a warm and humid ambient. The experimental arrangements used are described in the following sections.

Heat flow meter apparatus

The design of the heat flow meter apparatus was based on the ASTM guidelines [9] for such equipment. A schematic diagram of the experimental arrangement is shown in Fig. 1(a). The test insulation slab is placed between the smooth faces of the hot and cold plates which are squares of side 450 mm. These plates are essentially fin–tube heat exchangers built within thick brass plates. The heat exchangers are supplied with fluid from two constant temperature liquid baths, the temperatures of which are controlled automatically with an accuracy of 0.1°C.

Sandwiched between the faces of the test insulation specimen and the heat sink surfaces are two heat flux measuring pads. These include two heat flow meters which are located within a square cut out of a sheet of rubber with nominally the same thickness as the heat flow meter. The heat flow meters are square in shape with a side of 100 mm and thickness of 2 mm. The rubber sheet acts as a 'side guard' to reduce the lateral heat flow into the heat flow meter. A thin sheet of rubber is placed on either side of the heat flow meter to obtain good thermal contact with the heat sink surfaces and the insulation specimen. This helps

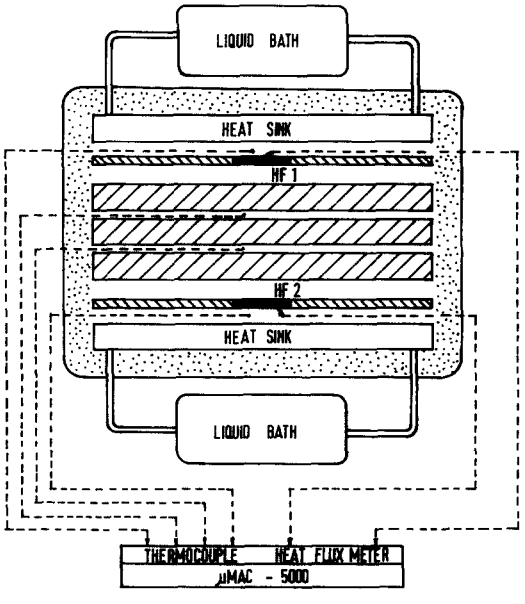

FIG. 1(a). Heat flow meter apparatus.

to reduce fluctuations in the heat flow meter output voltage which is sensitive to the thermal contact resistance on its surfaces. The use of two 'measuring pads' helps to determine the magnitude of the side heat losses and also the dynamic changes in the heat flow resulting from vapour migration and condensation when wet insulation specimens are tested. Thermocouples are located on each face of the measuring pads. The apparatus in this form is used to measure the thermal resistance and the thermal conductivity of dry insulations. The hot and cold plates are carried on cross bars. These have holes which are guided through four vertical threaded rods. This arrangement enables the adjustment to accommodate slabs of different thickness and also control the pressure applied to the insulation specimen. The entire assembly is surrounded with thick blocks of insulation which helps to achieve stable conditions rapidly.

The output voltages from the two heat flow meters and the various thermocouples are recorded through the appropriate interfaces in the μ-mac 5000 data acquisition and control system from Analog Devices Corporation. The experimental data is processed in an IBM-PC-AT computer which is interfaced to the μ-mac system.

The test procedure involved two important phases. These are: (a) calibration of the apparatus, (b) measurement of the dynamic variation of the thermal properties in the moist insulation specimen. In the calibration experiments, the thermocouples were separately calibrated using a temperature calibration set-up. The regression curve obtained was incorporated into the data analysis software used subsequently. The μ-mac system was calibrated to operate at the point which gives the best linearity between the transducer input voltage and the μ-mac output voltage. The temperature correction curves of the heat flow meters were also included in the data analysis software. The complete apparatus including the data acquisition system was calibrated using a standard insulation test specimen from the National Bureau of Standards of U.S.A. [10]. The thermal resistance measured in these tests were useful in establishing the accuracy of the calibration curve for the heat flow meters.

A series of tests were undertaken to measure the thermal conductivity and the thermal resistance of fibreglass slabs. The slabs were subsequently used to study the effect of water vapour migration and condensation on the thermal properties of insulation. In wet tests, water is sprayed on to one surface of the test specimen which is assembled in three or five layers with thermocouples sandwiched in interfaces between the layers. The total thicknesses of the slabs tested are 40 and 66 mm. The weight of water added is determined by measuring the increase in weight of the test specimen. The water is sprayed with the help of an atomizer which ensures a reasonably uniform spread of the water on the surface of the insulation. The wet specimen is then placed in a plastic bag and it is sealed to prevent the exchange of moisture with the surroundings. The preparation of this wet specimen required considerable care. Experience on the method of preparation was gained by performing a series of exploratory tests until consistent results were obtained. The heat flow meter apparatus is allowed to reach steady conditions at the preset hot and cold bath temperatures, with a 'dummy' specimen in position. At the start of the proper wet sample test, the dummy specimen is replaced with the wet test specimen. The output of the heat flow meters and thermocouples are continuously monitored until steady conditions are attained in the test specimen.

In a series of separate tests, the rate of condensation of moisture in the different layers of the slab was measured by removing the test sample from the apparatus at different times. After the measurement of the weight of the layers, that particular test was terminated and a new test was started with the same quantity of water on the wet face. This test was similarly terminated at a later time. By this procedure it was possible to obtain the history of the vapour condensation process for a given set of conditions at the hot and cold plates and for a given initial moisture content at the hot face. Attempts to remove the test sample from the apparatus and thus measure the condensation rate continuously did not prove satisfactory due to changes which occur during the measurement process.

Environmental chamber based heat flow meter system

The heat flow meter apparatus described in the previous section was used to study the vapour migration and condensation in insulation slabs where water is sprayed on to the hot face at the beginning of a test. However, in some practical situations water vapour ingress may occur from the warm ambient surrounding the insulation. This situation is simulated in an environmental chamber based heat flow meter system.

A schematic diagram of this experimental arrangement is shown in Fig. 1(b). The 'measuring pad', the cold plate, and the thermocouples with the associated data logging system are now assembled on the top face of the test section, as shown in Fig. 1(b). The test section is part of a closed-loop environmental chamber which is provided with an electric heater, a humidifier and a blower to circulate the air. The test section has a rectangular cross-section of 1.0×0.48 m and it is instrumented to measure the temperature and the relative humidity. The relative humidity is measured with a Vaisala humidity sensor and resistance temperature transducers are used to measure the temperature of the air in the test section at two locations. The humidifier is controlled automatically using the output of the relative humidity sensor which has a sensitivity of $\pm 2\%$. This arrangement was capable of maintaining the relative humidity of the air in the chamber within $\pm 1.0\%$ at high humidity levels of about 95%. The fluctuation of relative humidity

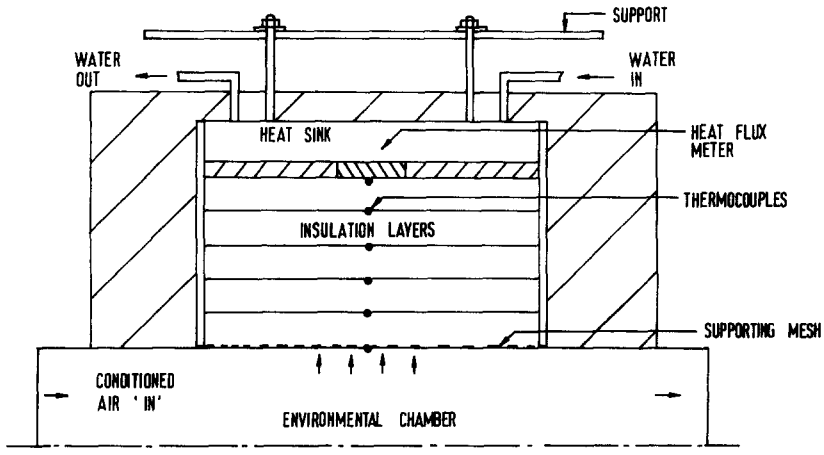

FIG. 1(b). Environmental chamber based heat flow meter system.

within the chamber was $\pm 5\%$ at lower humidities of about 70%.

The dry insulation slab, which was made up of five layers, had a total thickness of 66 mm. The slab is weighed and placed in a plastic cover with a square opening of side 360 mm on one face. The exposed face of the slab is placed on a thin wire mesh which is mounted flush with the top side of the test section. The mesh helps to prevent the sagging of the insulation slab and to obtain good contact between the five layers. The heat flow meter 'measuring pad' is sandwiched between the top surface of the insulation slab and the cold plate. Copper–constantan thermocouples are located at the interfaces of the insulation layers. The output of the thermocouples and the heat flow meter is connected to the data logging system described previously.

The experimental procedure to determine the variation of the temperature distribution within the slab, the heat flux and the rate of condensation of moisture in the different layers is similar to that described in the foregoing section. The duration of the test runs varied from about 12 to 60 h, which was sufficient to reach the quasi-steady phase of the transport process. Before the commencement of a test, the environmental chamber conditions are first stabilized using a 'dummy' insulation specimen.

In the next section of the paper, simple physical models are developed to simulate the experiments described above.

ANALYSIS

The physical processes which occur within the insulation slab during the two experiments described in the previous section are somewhat similar. They are governed by the same conservation equations of mass and energy, but the boundary conditions are different. A numerical solution of the time-dependent transport equations is available in ref. [14]. This analysis requires detailed physical properties of the insulation slab. These are not readily available. Moreover, for the duration of the tests reported in the present study, a large part of the transport process is in a quasi-steady state. Therefore, a simple analytical model is developed to interpret mainly the quasi-steady results.

The following assumptions, which are similar to those made by Ogniewicz and Tien [12] and Motakef and El-Masri [13] in their analyses, are made in the present physical model.

(1) The vapour and heat fluxes are given by Fick's law and Fourier's law, respectively.

(2) Condensation of liquid occurs when the vapour concentration at any location exceeds the saturation concentration corresponding to the local temperature. The functional dependence of the saturation concentration on temperature is given by the Clausius–Clapeyron relationship.

(3) For the physical conditions in the present experiments, the liquid formed is in a pendular state and does not, therefore, diffuse.

(4) There are no convective contributions to heat and mass transport.

(5) Gravitational effects are negligible.

(6) The physical properties of the system are uniform.

The governing equations of mass and energy may be written as

$$\frac{\partial}{\partial z}\left[\rho_a D_0 \frac{\partial C}{\partial z}\right] - \Gamma = \rho_a \frac{\partial C}{\partial t} \tag{1}$$

$$\frac{\partial}{\partial z}\left[k \frac{\partial T}{\partial z}\right] + \Gamma h_{fg} = \rho c \left(\frac{\partial T}{\partial t}\right). \tag{2}$$

where Γ represents the rate of condensation of liquid. Solutions to equations (1) and (2) which are applicable to the experimental conditions described previously are now obtained.

Moisture introduced at one face

A reference to the measured heat flux variation depicted in Fig. 4 for this situation shows that there

are three identifiable phases of the moisture transport process. Following a short transient, the heat flux and temperature reach a quasi-steady state. As the moisture content at the hot face of the slab is depleted to a low level, a second transient period during which the hot face dries up is observed. This is followed by the final steady state where most of the moisture has condensed at the cold face.

In the present analysis, attention is concentrated on the first quasi-steady state where the heat flux is the largest and is, therefore, of considerable practical interest. The vapour during this phase is in a saturated state and there is no dry region in the slab. The concentration is related to the temperature by the Clausius–Clapeyron equation given by

$$C^*(T) = \bar{C}\,e^{a(1/T_0 - 1/T)} = g(T). \tag{3}$$

For the temperature range of about 0–58°C, which was used in the present experiments, the constants in equation (3) obtained at the mean temperature are

$$T_0 = 301\ \text{K}$$

$$a = 5271.2$$

and

$$\bar{C} = 0.0232. \tag{4}$$

The two faces of the slab are in a saturated condition during this quasi-steady state. Therefore, the boundary conditions are

$$\text{at } z = 0, \quad T(0) = T_1 \quad \text{and} \quad C(0) = g(T_1) \tag{5}$$

$$\text{at } z = L, \quad T(L) = T_2 \quad \text{and} \quad C(L) = g(T_2). \tag{6}$$

The combination of equations (1)–(3) for the quasi-steady state gives

$$\frac{\mathrm{d}}{\mathrm{d}z}\left\{[k + h_{fg}\rho_a D_0 g'(T)]\frac{\mathrm{d}T}{\mathrm{d}z}\right\} = 0 \tag{7}$$

where $g'(T) = \mathrm{d}g/\mathrm{d}T$.

Integrating equation (7) and applying boundary conditions (5) and (6), the temperature distribution is obtained as

$$k(T - T_1) + h_{fg}\rho_a D_0[g(T) - g(T_1)] = k\frac{(T_2 - T_1)z}{L} + h_{fg}\rho_a D_0\frac{[g(T_2) - g(T_1)]z}{L}. \tag{8}$$

The total heat flux, vapour flux and the equivalent thermal conductivity are given by

$$q(z) = \frac{k(T_2 - T_1)}{L} + h_{fg}\rho_a D_0\frac{[g(T_2) - g(T_1)]}{L} \tag{9}$$

$$\phi(z) = -\frac{D_0\rho_a g'(T)q(z)}{[k + h_{fg}\rho_a D_0 g'(T)]} \tag{10}$$

and

$$k_e = k + h_{fg}\rho_a D_0 g'(T). \tag{11}$$

Equations (8)–(10) are used to obtain the temperature distribution, the heat flux and the vapour flux distribution in the slab and these are compared with the experimentally measured quantities. The variation of the equivalent thermal conductivity of the slab is obtained from equation (11). The physical properties of the system, which are used in the computation, are given in the next section.

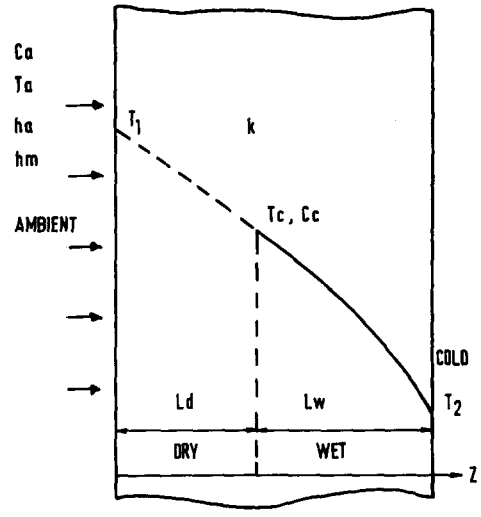

FIG. 2. Schematic diagram of slab.

Moisture absorption from the ambient

The variation of the heat flux and temperature for this boundary condition during the time period considered in the present experiments is shown in Fig. 11. It is seen that a quasi-steady state is reached after a short initial transient variation. The physical situation for the slab is depicted in Fig. 2. In general, the slab has a dry region close to the exposed surface and a wet region which extends up to the cold plate. The analysis of the two regions is considered separately.

In the dry region, the governing equations (1) and (2) are uncoupled because the condensation rate $\Gamma = 0$. At the dry–wet boundary, the concentration C is given by the Clausius–Clapeyron relationship. The temperature and concentration gradients at the dry–wet interface are obtained by considering the dry region of the slab and the surrounding ambient.

These are given by

$$\left.\frac{\mathrm{d}T}{\mathrm{d}z}\right|_c = \frac{(T_c - T_a)}{L_d}\frac{1}{(1 + k/L_d h_a)} \tag{12}$$

$$\left.\frac{\mathrm{d}C}{\mathrm{d}z}\right|_c = \frac{(C_c - C_a)}{L_d}\frac{1}{\left(1 + \dfrac{\rho_a D_0}{L_d h_m}\right)}. \tag{13}$$

But

$$\left.\frac{\mathrm{d}C}{\mathrm{d}z}\right|_c = g'(T_c)\left.\frac{\mathrm{d}T}{\mathrm{d}z}\right|_c. \tag{14}$$

The combination of equations (12)–(14) gives

$$\left[\frac{L_d+\frac{\rho_a D_0}{h_m}}{L_d+\frac{k}{h_a}}\right]=\left(\frac{C_a-C_c}{T_a-T_c}\right)\frac{1}{g'(T_c)}. \quad (15)$$

The temperature and concentration distributions within the dry region of the slab are linear and these are easily obtained by solving equations (12) and (13).

The governing equation for the wet region is the same as equation (7), but the boundary conditions for this case are somewhat different. Assuming $z = 0$, at the dry–wet interface, the boundary conditions can be written as

$$\text{at } z=0, \quad T(0)=T_c \quad \text{and} \quad \left.\frac{dT}{dz}\right|_{z=0}=\left.\frac{dT}{dz}\right|_c \quad (16)$$

at $z = L_w$, the slab is in a saturated condition and $T(L_w) = T_2$.

By solving equation (7), with boundary conditions (16), the temperature distribution in the wet region is obtained as

$$k(T-T_c)+h_{fg}\rho_a D_0[g(T)-g(T_c)] = [k+h_{fg}\rho_a D_0 g'(T_c)]\frac{(T_c-T_a)\left(\frac{z}{L_d}\right)}{\left[1+\frac{k}{L_d h_a}\right]}. \quad (17)$$

The solution of equations (15) and (17) cannot be obtained directly because the lengths of the dry region L_d and the wet region L_w are as yet unknown. The following trial and error procedure is, therefore, adopted.

An initial trial value is assumed for the dry–wet interface temperature T_c. The corresponding concentration C_c is computed from the Clausius–Clapeyron relationship (3). These values are substituted in equation (15) to obtain the dry region length, L_d. The wet region length, L_w, is given by z in equation (17) when $T = T_2$. The total slab length, L, is then obtained from $L = (L_d + L_w)$. The computed length, L, is compared with the actual slab length and the value of T_c is adjusted until the computed length matches the slab length. The temperature distribution within the slab, the heat flux and the condensation rate are obtained directly using equations (17), (9) and (10), respectively.

The complete calculation requires several physical properties of the system. Typical values used for these are given in Table 4.

The diffusion coefficient for the water vapour–air mixture in the fibrous slab is obtained from the following formula [15]:

$$D_a = 1.97\times10^{-5}\left(\frac{T_m}{255.2}\right)^{1.685} \quad (18)$$

and

$$D_0 = D_a\frac{\varepsilon_v}{\tau}$$

where ε_v is the void fraction, τ the tortuosity factor and T_m the mean temperature of the slab. The heat transfer coefficient, h_a, is estimated experimentally while the mass transfer coefficient, h_m, is deduced from the mass transfer analogy [15] as

$$h_m = \left(\frac{h_a}{1.047}\right)\left(\frac{\rho_a D_a}{k_a}\right). \quad (19)$$

RESULTS AND DISCUSSION

The various transducers used and the experimental procedure adopted introduced several uncertainties to the measured quantities. The calibration curve supplied by the manufacturer of the heat flow meter was checked by measuring the thermal conductivity of the standard insulation specimen [10] over the temperature range of interest. There was a maximum deviation of about 6%. The temperature calibration curve of the heat flow meter was, therefore, adjusted to obtain agreement with the results of the standard specimen. For the tests reported in this study, the heat exchange at the outer edge of the apparatus is estimated to be less than 1% of the measured heat flow, in the quasi-steady state. This is due to the thick polystyrene insulation used and the relatively small difference between the temperature of the ambient and the mean temperature of the insulation slab.

The thermal conductivity vs temperature curve of the standard specimen is known to have an accuracy of about 2%. The thermocouples and the associated data logging system were calibrated to an accuracy of 0.1°C.

The measurement of the condensation rate in the insulation layers involved two sources of uncertainty. Although the mass of condensate was measured with an electronic balance with an accuracy of 0.01%, there was a maximum discrepancy of about 4% between the initial mass of water added and the sum of the masses of the water condensed in the different layers at the end of the test. The maximum uncertainty in the slope of the condensation curve (Fig. 5) was about 5%. The combined uncertainty of the measured condensation rate is estimated to be less than about 7%. A series of tests were performed to determine the effect of the interfacial resistance between the layers. This was found to have a negligible effect on the dry state thermal conductivity of the slab. However, at the end of each wet test, when the different layers are weighed, there is some uncertainty due to the water deposited in the interfaces. This causes some scatter in the condensation vs time plot. The results obtained with the two experimental arrangements are discussed in the following sections.

Moisture introduced at one face

The heat flow meter measurements were carried out for five sets of values of the hot and cold plate

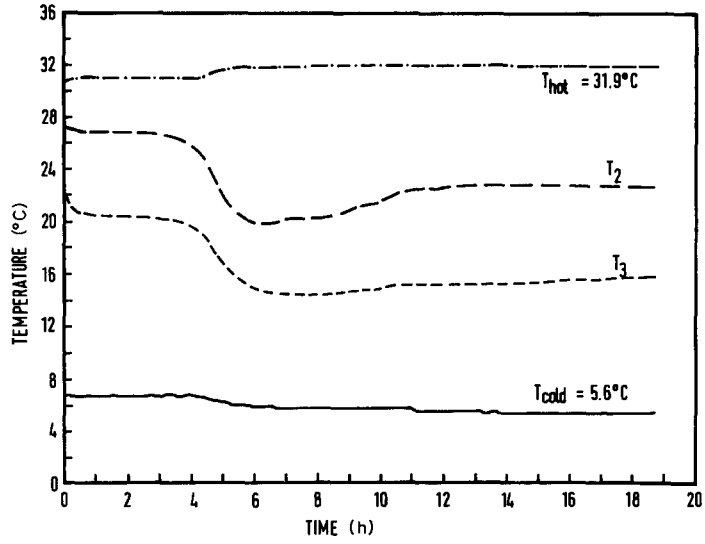

FIG. 3. Variation of temperature with time. Conditions: $\rho_{slab} = 53$ kg m^{-3}, $L = 40$ mm.

temperatures and three values of the initial moisture level in the slab. A typical temperature history for a three-layer slab is shown in Fig. 3. The corresponding variation of the heat flux is depicted in Fig. 4. The physical processes which occur can be explained by referring to these temperature and heat flux histories.

Following a short initial transient after the slab is placed in the apparatus, the temperature and heat flux reach a quasi-steady phase which lasts from about 1 to 5 h. The duration of this phase depends on the initial moisture content in the slab and the temperature of the hot face. Water evaporates at the hot face and condenses at the cold face during this phase and the vapour throughout the slab is in a saturated condition. As time proceeds, the quantity of liquid at the hot face is reduced and a 'dry out' begins to occur. This corresponds to the transient variation seen in Fig. 3, from about 4 h to about 12 h. A similar transient period is observed in the heat flux shown in Fig. 4. At the end of the transient period, most of the liquid is at the cold face, and the temperature and heat flux reach the final steady state. The thermal conductivity of the slab at this stage is very close to the dry value. The presence of a liquid layer adjacent to the cold face seems to have little effect on the variation of the heat flux and temperature. The slight decrease in hot face temperature and the slight increase in the cold face temperature during the quasi-steady state (Fig. 3) is due to the temperature drop across the heat flow meters. These are larger when the heat flux is at the

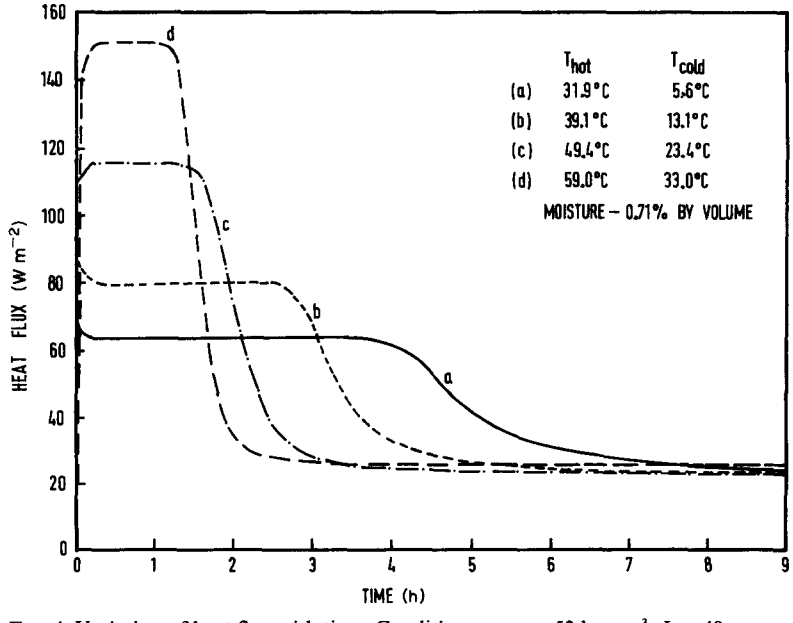

FIG. 4. Variation of heat flux with time. Conditions: $\rho_{slab} = 53$ kg m^{-3}, $L = 40$ mm.

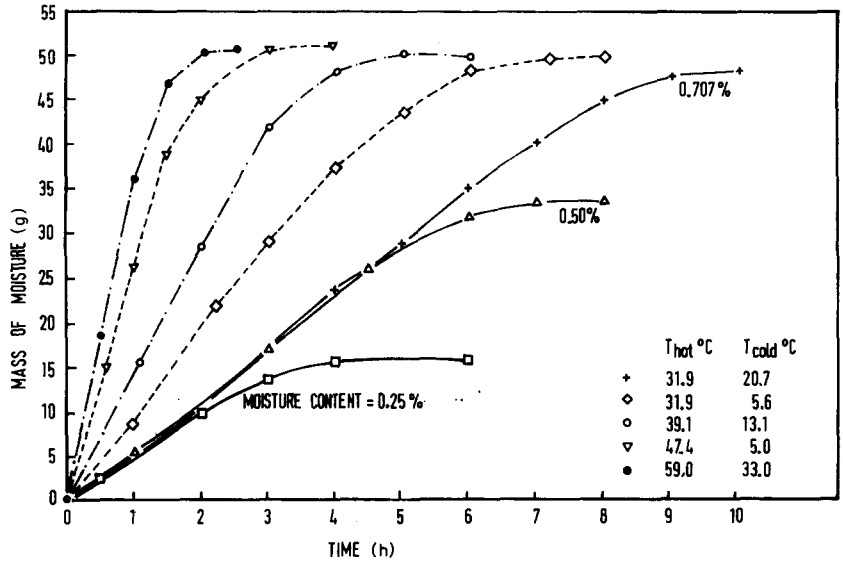

FIG. 5. Variation of the mass of condensate in the cold layer with time. Conditions: $\rho_{slab} = 53$ kg m^{-3}, $L = 40$ mm.

quasi-steady value. The heat flux variations shown in Fig. 4 reach nearly the same final value because these curves are for the same temperature difference between the faces. The results obtained for all the test conditions show similar trends of behaviour.

The rate of condensation of water in the insulation layers is obtained by weighing them at different times during experiments. The variation in the mass of water in the layer adjacent to the cold plate is shown in Fig. 5. This is the layer which has the largest amount of water. It should be noted that the condensation rate within the insulation layer is relatively small. Most of the water condenses at the cold face, because the plate is impermeable to water vapour. This condensate is usually deposited in the adjacent layer of insulation. The vapour flux entering the insulation layer adjacent to the cold face is given by the slope of the curves in Fig. 5. It is interesting to note that during the quasi-steady phase of the vapour transport process, the slope is nearly constant indicating that the vapour flux is constant during this period. It is seen from Fig. 5 that the vapour flux during the quasi-steady phase is almost independent of the initial moisture content of the slab, when the hot and cold face temperature are the same. The vapour flux, however, increases with the increase in the mean slab temperature and the temperature difference between the faces.

The calculated and measured temperature distributions within the slab for two different thicknesses and a series of hot and cold face temperatures are shown in Figs. 6 and 7. There is good agreement for the thicker slab while there is some discrepancy for the thinner slab. One of the main difficulties of this measurement is the determination of the exact position of the thermocouple. This uncertainty arises due to the soft nature of the fibreglass layers. It should be noted that 0.1 in the (z/L) scale of Fig. 7, represents a physical distance of 4 mm. The measured temperature distribution for the thicker slab is more accurate as five measuring points were used for this case. The temperature distributions become more curved when the temperature difference between the faces and the mean temperature are increased.

The distribution of the measured and calculated dimensionless vapour flux in the slab during the quasi-steady state is shown in Fig. 8. There is satisfactory

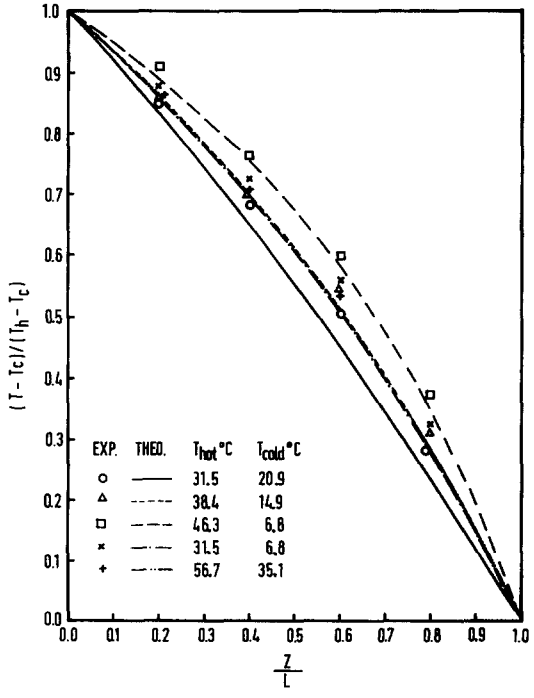

FIG. 6. Quasi-steady temperature distribution in the slab. Conditions: $\rho_{slab} = 53$ kg m^{-3}, $L = 66$ mm.

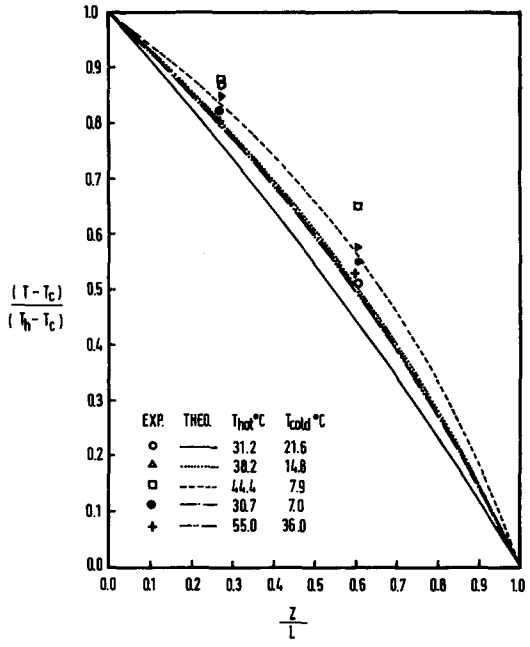

FIG. 7. Quasi-steady temperature distribution in the slab. Conditions: $\rho_{slab} = 53$ kg m^{-3}, $L = 40$ mm.

agreement between the measured and calculated distributions. The slope of these curves gives the condensation rate, which increases continuously from the hot to the cold face of the slab. The results are similar for the two slab thicknesses, when the temperature conditions are the same.

The calculated and measured values of the heat flux and the vapour flux entering the insulation layer adjacent to the cold plate are given in Tables 1 and 2, for the two slab thicknesses. Equations (9) and (10) were used for these calculations. There is satisfactory agreement between the measurements and the computed values. The range of typical values of the physical properties used for the computation are listed in Table 4. These are obtained from several sources. The dry thermal conductivity of the slab was measured while the density and the latent heat were obtained from property tables. All physical properties were assumed constant and they are evaluated at the mean slab temperature.

The distribution of the equivalent thermal conductivity of the slab is shown in Figs. 9 and 10. Equation (11) shows that this is essentially a function of the local temperature. However, the equivalent thermal conductivity has the spatial dependence shown in Fig. 10, which is almost linear. It is seen that the equivalent thermal conductivity increases both with the mean slab temperature and the temperature difference between the faces of the slab. Its magnitude varies from about 2 to 13 times the dry thermal conductivity.

Moisture absorption from the ambient

The temperature and the heat flux variation in the slab when it absorbs moisture from the ambient are shown in Fig. 11. For the time period of about 60 h, which was the duration of the present series of experiments, the temperature and heat flux are in a quasi-steady state. However, this situation may change when more liquid is condensed in the slab.

The slab in this case has a dry region from the exposed surface to an interface at which the vapour concentration is equal to the saturation concentration corresponding to the local temperature. The slab thickness from this interface to the cold surface is saturated with vapour and continuous condensation occurs. The condensation rate is largest at the cold face because the plate is impermeable to water vapour.

The tests in this case were carried out for three values of the ambient humidity and the results are summarized in Fig. 12 and Table 3. There is good agreement between the measured and calculated temperature distributions within the slab as seen in Fig. 12. The computed dry–wet interface is also indicated in the figure. The computation for this case involves two additional physical parameters. These are the heat

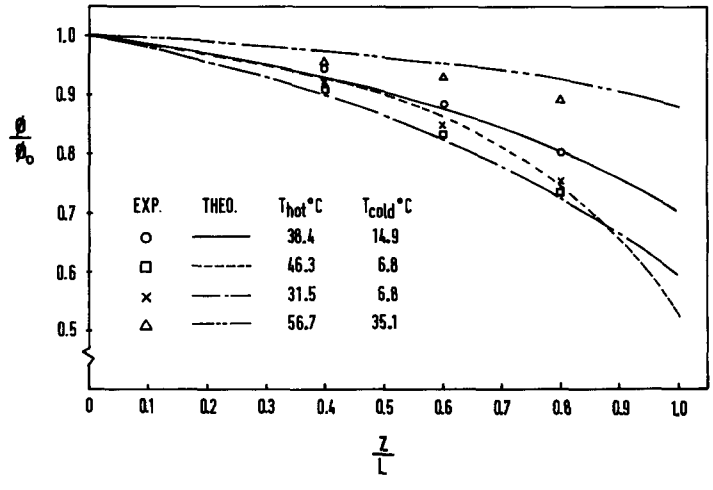

FIG. 8. Quasi-steady vapour flux distribution in the slab. Conditions: $\rho_{slab} = 53$ kg m^{-3}, $L = 66$ mm.

Table 1. Measured and calculated quasi-steady heat flux and vapour flux for slab thickness, $L = 66$ mm

T_{hot}(°C)	T_{cold}(°C)	Heat flux (W m^{-2}) Measured	Calculated	Vapour flux (kg s^{-1} m^{-2}) Measured	Calculated
38.4	14.9	49.4	46.8	1.47×10^{-5}	1.53×10^{-5}
31.5	6.8	37.1	36.5	1.02×10^{-5}	1.10×10^{-5}
46.3	6.8	88.0	83.8	2.59×10^{-5}	2.91×10^{-5}
56.7	35.1	99.5	99.2	4.15×10^{-5}	3.71×10^{-5}
31.5	20.9	19.8	20.1	0.59×10^{-5}	0.62×10^{-5}

Table 2. Measured and calculated quasi-steady heat flux and vapour flux for slab thickness, $L = 40$ mm

T_{hot}(°C)	T_{cold}(°C)	Heat flux (W m^{-2}) Measured	Calculated	Vapour flux (kg s^{-1} m^{-2}) Measured	Calculated
55	36	148.0	140.5	6.2×10^{-5}	5.30×10^{-5}
44.4	7.9	140.0	124.0	4.3×10^{-5}	4.10×10^{-5}
30.7	7.0	58.5	56.9	1.66×10^{-5}	1.62×10^{-5}
31.2	21.6	32.8	30.2	1.01×10^{-5}	0.92×10^{-5}
38.2	14.8	78.9	76.3	2.3×10^{-5}	2.43×10^{-5}

and mass transfer coefficients at the exposed surface. The flow pattern within the test section is not completely known and the use of free convection correlations to compute the heat transfer coefficient did not give satisfactory results. The mean air speed in the test section was about 0.15 m s^{-1}. Separate experiments were, therefore, performed to determine the heat transfer coefficients under the same conditions of flow in the test chamber as for the above wet tests.

For these tests, the cold plate temperature was increased and the humidity in the chamber was maintained at a low value to prevent condensation. The

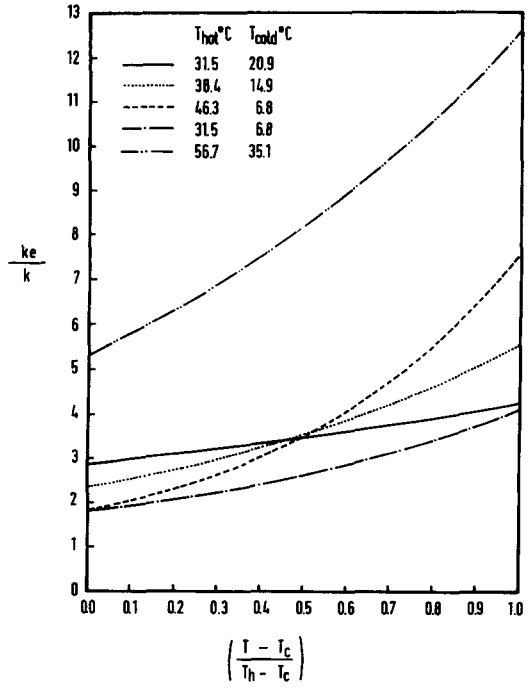

FIG. 9. Variation of dimensionless equivalent thermal conductivity with dimensionless temperature. Conditions: $\rho_{slab} = 53$ kg m^{-3}, $L = 66$ mm.

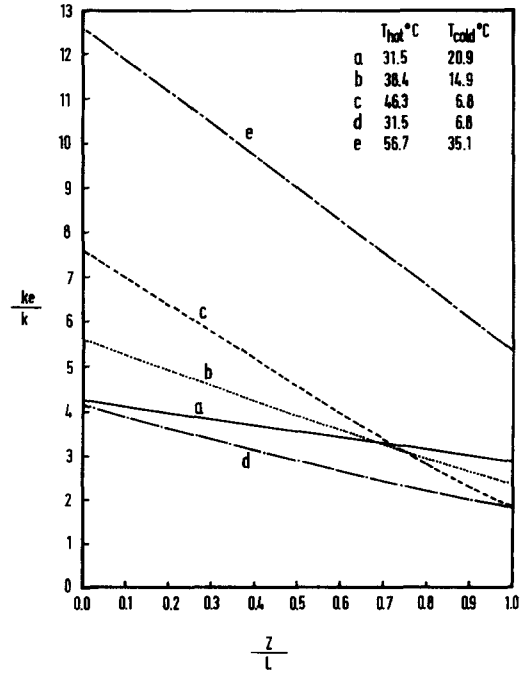

FIG. 10. Distributions of dimensionless equivalent thermal conductivity in the slab. Conditions: $\rho_{slab} = 53$ kg m^{-3}, $L = 66$ mm.

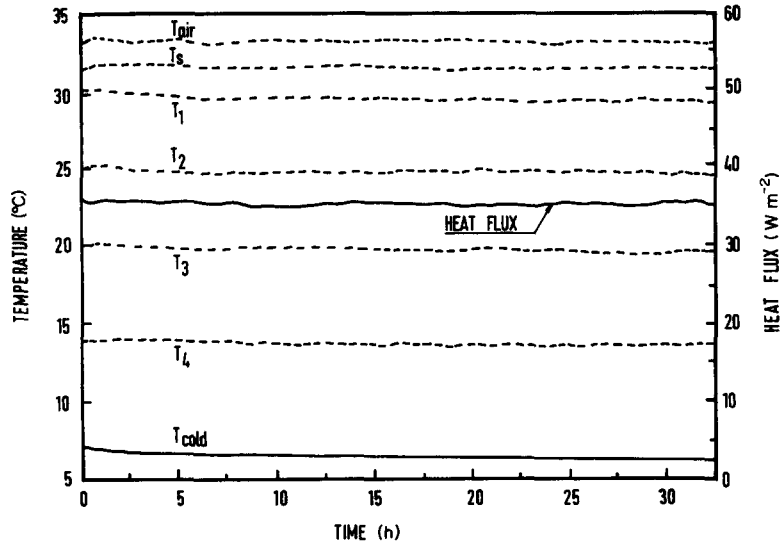

FIG. 11. Variation of temperature and heat flux in the slab exposed to the ambient. Conditions: $\rho_{slab} = 53\ kg\ m^{-3}$, $L = 66$ mm.

temperature distribution within the slab is linear under these conditions. The measured dry thermal conductivity of the slab and the temperature distribution were used to compute the heat flux within the slab and the surface temperature. This information was then used to estimate the heat transfer coefficient at the exposed surface by a simple heat balance. The value thus obtained was well above the free convection heat transfer coefficient. The mass transfer coefficient was determined by the application of the mass transfer analogy [15].

The sensitivity of the computed quantities, namely the heat flux, the vapour flux entering the cold layer and the temperature of the mid-section was examined by varying the properties about the baseline value. The results are summarized in Table 4. The baseline values, indicated in parentheses, are evaluated at the mean temperature of the slab. The effect of the heat

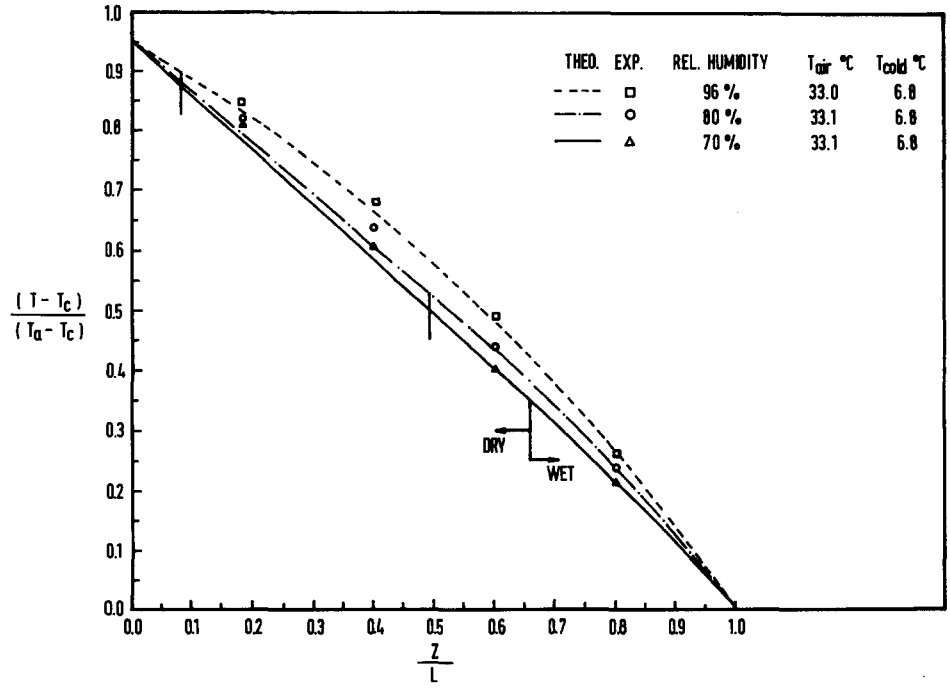

FIG. 12. Quasi-steady temperature distribution in the slab exposed to the ambient. Conditions: $\rho_{slab} = 53\ kg\ m^{-3}$, $L = 66$ mm.

Table 3. Measured and calculated heat flux and vapour flux for slab thickness, $L = 66$ mm

$T_{ambient}$(°C)	Relative humidity (%)	T_{cold}(°C)	Heat flux (W m^{-2}) Measured	Calculated	Vapour flux (kg s^{-1} m^{-2}) Measured	Calculated
33.0	96	6.8	35.0	36.7	0.92×10^{-5}	0.85×10^{-5}
32.0	90	6.8	32.0	33.7	0.76×10^{-5}	0.77×10^{-5}
33.1	80	6.8	30.2	32.5	0.69×10^{-5}	0.74×10^{-5}
33.2	70	6.8	27.4	29.5	0.58×10^{-5}	0.65×10^{-5}

Table 4. Sensitivity of the computed quantities to uncertainties in physical properties (baseline values in parentheses)

Property varied	Property magnitude	Heat flux (W m^{-2})	Vapour flux (kg s^{-1} m^{-2})	Dimensionless temperature of mid-section (°C)
h_a (W m^{-2})	5	35.90	0.825×10^{-5}	0.56
(6.9)	9	37.13	0.85×10^{-5}	0.57
k (W m^{-1} K^{-1})	0.032	35.96	0.85×10^{-5}	0.57
(0.034)	0.036	37.40	0.84×10^{-5}	0.56
ρ_a (kg m^{-3})	1.15	35.74	0.81×10^{-5}	0.57
(1.20)	1.25	37.62	0.88×10^{-5}	0.58
ε_v	1.0	37.62	0.875×10^{-5}	0.58
(0.96)	0.90	35.26	0.79×10^{-5}	0.57
D_a (m^2 s^{-1})	2.25×10^{-5}	34.54	0.76×10^{-5}	0.57
(2.49×10^{-5})	2.75×10^{-5}	39.06	0.93×10^{-5}	0.57
Properties at baseline value		36.72	0.85×10^{-5}	0.57

transfer coefficient, the dry state thermal conductivity and the density is within the uncertainty of the measurements. The diffusion coefficient and the void fraction have a significant effect on the computed vapour flux but their effect on the heat flux and the temperature is smaller.

As expected, the computed length of the wet region increases with increasing ambient humidity and the temperature distribution becomes more curved. There is satisfactory agreement between the calculated and measured heat flux and condensation rate as seen in Table 3. These quantities also increase with increasing ambient humidity. The distribution of the computed dimensionless vapour flux in the slab and some experimental data are shown in Fig. 13. The vapour flux begins to decrease from unity at the dry–wet interface. The slope of these curves is the rate of condensation of vapour. This increases progressively until the cold plate is reached.

Work is currently in progress to increase the testing

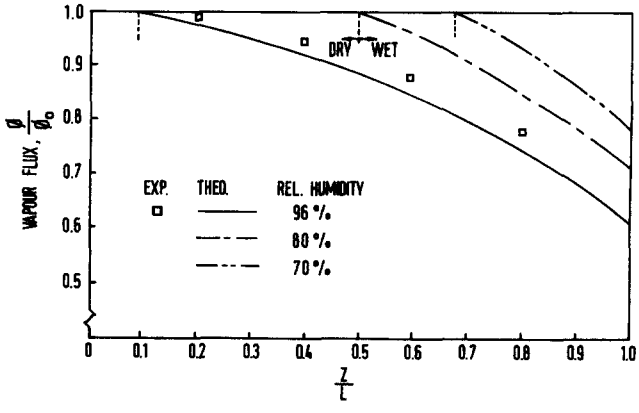

FIG. 13. Quasi-steady vapour flux distribution in the slab exposed to the ambient. Conditions: $\rho_{slab} = 53$ kg m^{-3}, $L = 66$ mm, $T_a = 33.0$°C, $T_{cold} = 6.8$°C.

time to include the diffusion of the liquid phase from the cold side of the insulation slab.

CONCLUSION

An experimental study of the diffusion and condensation of water vapour in fibrous insulations under two different boundary conditions is reported. These situations have considerable practical relevance in air conditioning applications. The simple quasi-steady models developed for the two sets of conditions predict the temperature distributions, the heat flux and the vapour flux satisfactorily. The equivalent thermal conductivity of the slab in the presence of condensation has a linear distribution. The magnitude of the equivalent thermal conductivity increases with increasing mean slab temperature and temperature difference.

Acknowledgements—The authors acknowledge with gratitude a grant awarded under the ASEAN–Australia Economic Cooperation Programme in support of the work on thermal insulation.

REFERENCES

1. W. J. Batty, P. W. O'Callagham and S. D. Probert, Corrosion under insulants, *Appl. Energy* **16,** 239–247 (1984).
2. H. B. Jespersen, Thermal conductivity of moist materials and its measurement, *J. Inst. Heat. Vent. Engrs* **21,** 216–222 (1953).
3. F. A. Joy, *Symposium on Thermal Conductivity Measurements and Applications of Thermal Insulations*, ASTM STP 217, pp. 65–80. American Society of Testing and Materials (1957).
4. W. Woodside, Probe for thermal conductivity measurements of dry and moist materials, *Heat. Pip. Air Condit.* **30,** 163–170 (1958).
5. C. Langlais, M. Hyrien and S. Klarsfeld, *Moisture Migration in Building*, ASTM STP 779, pp. 191–206. American Society for Testing and Materials (1982).
6. W. C. Thomas, G. P. Bal and R. J. Onega, *Heat and Mass Transfer in a Glass Fiber Roof Insulating Material*, ASTM STP 789, pp. 582–601. American Society of Testing and Materials (1983).
7. C. Langlais and S. Klarsfeld, Heat and mass transfer in fibrous insulation, *J. Thermal Insulation* **8,** 49–80 (July 1984).
8. D. K. Modi and S. M. Benner, Moisture gain of spray-applied insulations and its effect on effective thermal conductivity, Part I, *J. Thermal Insulation* **8,** 259–277 (April 1985).
9. ASTM-C518, Steady-state thermal transmission properties by heat flow meter method. ASTM, Philadelphia (1976).
10. B. G. Rennex, R. R. Jones and D. G. Ober, Development of calibrated transfer specimens of thick low-density insulations, *Proc. Int. Thermal Conductivity Conf.*, Gaithersburg, pp. 419–426 (15–18 June 1981).
11. N. E. Wijeysundera, M. N. A. Hawlader, Ong Sin Gee and U. Kyaw Sein, Thermal property measurement of wet and dry insulations, Energy Conservation Technology Seminar, National University of Singapore, Singapore, pp. 9.1–9.19 (12 September 1986).
12. Y. Ogniewicz and C. L. Tien, Analysis of condensation in porous insulation, *Int. J. Heat Mass Transfer* **24,** 421–429 (1983).
13. S. Motakef and M. A. El-Masri, Simultaneous heat and mass transfer with phase change in a porous slab, *Int. J. Heat Mass Transfer* **29,** 1503–1512 (1986).
14. K. Vafai and S. Sarkar, Condensation effects in a fibrous insulation slab, *Trans. ASME, J. Heat Transfer* **108,** 667–675 (1986).
15. D. K. Edwards, V. E. Denny and A. F. Mills, *Transfer Processes*. McGraw-Hill, New York (1976).

DIFFUSION DE VAPEUR D'EAU ET CONDENSATION DANS DES ISOLANTS FIBREUX

Résumé—On décrit une étude expérimentale de la diffusion et de la condensation de la vapeur d'eau dans des plaques d'isolant en fibre de verre. Dans la première série d'expériences, l'eau est pulvérisée sur la face chaude de la plaque et on utilise un appareil fluxmétrique thermique. Dans la seconde série, l'une des faces de la plaque est exposée à une ambiance chaude et humide et l'autre face est maintenue à une température basse. Des modèles analytiques simples sont développés pour la phase quasi permanente du mécanisme de condensation dans les deux expériences. La distribution calculée de température, le flux de chaleur et le flux de vapeur s'accordent bien avec les mesures.

DIFFUSION UND KONDENSATION VON WASSERDAMPF IN FASERIGEN WÄRMEDÄMMUNGEN

Zusammenfassung—Eine experimentelle Untersuchung der Diffusion und Kondensation von Wasserdampf in Wärmedämmplatten aus Glasfasern wird vorgestellt. In einer ersten Versuchsserie wird Wasser auf die heiße Plattenoberfläche gesprüht und diese in einer Wärmestrommeßeinrichtung untersucht. In einer zweiten Versuchsserie wird eine Plattenoberfläche einer warmen und feuchten Umgebung ausgesetzt; die andere Oberfläche wird auf niedriger Temperatur gehalten. Einfache analytische Modelle werden für die quasistationäre Kondensation bei den beiden Experimenten entwickelt. Die Berechnungen für Temperaturverteilung, Wärmestrom und Dampfstrom stimmen gut mit den gemessenen Werten überein.

ДИФФУЗИЯ И КОНДЕНСАЦИЯ ВОДЯНОГО ПАРА В ВОЛОКНИСТЫХ ИЗОЛЯЦИОННЫХ МАТЕРИАЛАХ

Аннотация—Приводятся данные экспериментального исследования диффузии и конденсации водяного пара в изоляционных плитах из стеклянного волокна. В первой серии экспериментов вода распыляется по горячей поверхности плиты и затем проводятся термоанемометрические измерения. Во второй серии одна из сторон плиты контактирует с нагретой влажной окружающей средой, а противоположная поддерживается при низкой температуре. Разработаны простые аналитические модели квазистационарной фазы процесса конденсации в обоих экспериментах. Рассчитанные распределение температур, значения теплового потока и потока пара хорошо согласуются с результатами измерений.